Crystallization-Induced Lamellar-to-Lamellar Thermal Transition in Salt-Containing Block Copolymer Electrolytes

Wen-Shiue Young, Paul J. Brigandi, and Thomas H. Epps, III*

Department of Chemical Engineering, University of Delaware, Newark, Delaware 19716

Received June 23, 2008
Revised Manuscript Received July 28, 2008

Polymer electrolytes with suitable ionic conductivities and mechanical properties are necessary components for solid-state battery and fuel cell membranes.[1,2] While high ionic conductivity decreases the internal potential loss, adequate mechanical properties are required to prevent short-circuiting between electrodes and to reduce dendrite formation.[2−5] One promising polymer electrolyte for lithium ion conduction is poly(ethylene oxide) [PEO]; however, the mechanical properties of molten PEO, required to facilitate coordinated polymer chain motion and ion transport, are subpar.[5−8] To overcome this limitation, block copolymers containing PEO and complementary blocks have been employed to vary the morphological and mechanical properties.[9−21] The self-assembly of these copolymers permits the design of flexible, yet sturdy membranes containing conducting channels for ion transport. In addition to PEO-containing copolymers,[13,15−18,22,23] researchers have investigated salt doping effects in copolymer systems containing blocks such as PMMA or PVP.[24−26] For these systems, the domain spacings and/or order−disorder transition temperatures (T_{ODT}'s) increased significantly upon the addition of salt.

Most copolymer/salt doping has focused on the low salt concentration regime, analogous to ether oxygen to lithium cation ([EO]:[Li]) ratios ranging from 50:1 to 12:1; however, recent work by Bruce and co-workers has shown promise at higher salt concentrations.[27] Here, we summarize our experiments on lithium salt-doped poly(styrene-*b*-ethylene oxide) [PS−PEO] diblock copolymers with high salt content. The PS−PEO was obtained from Polymer Source and had a molecular weight of 14 500 g/mol ($M_w/M_n = 1.05$) and a PEO volume fraction of $f_{PEO} = 0.324$ (calculated using homopolymer densities at 140 °C).[28] Two salts, lithium perchlorate ($LiClO_4$) and lithium trifluoromethanesulfonate ($LiCF_3SO_3$), were used, at an [EO]:[Li] ratio of 3:1. While this composition is not commonly employed for conducting applications in molten PEO,[29−31] it is useful for tuning copolymer volume fraction and interactions.

In dealing with hygroscopic polymer electrolyte complexes, such as PEO:Li, it is important to ensure that moisture uptake does not influence the experimental results.[19,21,32] Thus, the diblock copolymer was dried under vacuum and placed in an argon-filled glovebox for all further sample handling. Our small-angle X-ray scattering (SAXS) sample cells were prepared and sealed in the glovebox, and all scattering experiments were conducted under vacuum. Transmission electron microscopy (TEM) samples were cut directly from samples examined on the SAXS using a cryo-ultramicrotome.

* To whom correspondence should be addressed. E-mail: thepps@udel.edu.

The morphology of the neat (nondoped) material was examined using SAXS and TEM (not shown), which showed a hexagonally packed cylindrical structure with a domain spacing of 13.9 nm and an order−disorder transition temperature (T_{ODT}) of ∼180 °C. The melting temperature (T_m) of the PEO domain was 41 °C.

The temperature-dependent scattering behavior of salt-doped PS−PEO was examined using SAXS. Parts a and b of Figure 1 show patterns for PS−PEO:$LiClO_4$ and PS−PEO:$LiCF_3SO_3$, respectively, upon cooling. At temperatures ranging from 202 to 157 °C, the $LiClO_4$-doped sample exhibits a lamellar nanostructure with Bragg reflections located at q^*, $2q^*$, $3q^*$, and $4q^*$ (q^* is the primary scattering peak). The change in morphology from cylinders (neat sample) to lamellae (doped sample) is not unexpected and likely results from increased chain stretching in the PEO block.[17,22,23,26] A domain spacing of 23.3 nm is calculated from q^* at 157 °C. As the sample is cooled below 157 °C, the growth of a second series of peaks, corresponding to a larger characteristic length scale, is observed (indicated by arrows on the 138 °C−1 h trace). These smaller q peaks grow at the expense of the higher temperature peaks that exist above 157 °C. After extended annealing the larger q series completely disappears, and a single series of peaks is located, as shown in the 120 °C trace. Again, Bragg reflections of q^*, $2q^*$, $3q^*$, and $4q^*$ are found, indicative of a lower temperature lamellar structure. Thus, a transition from one

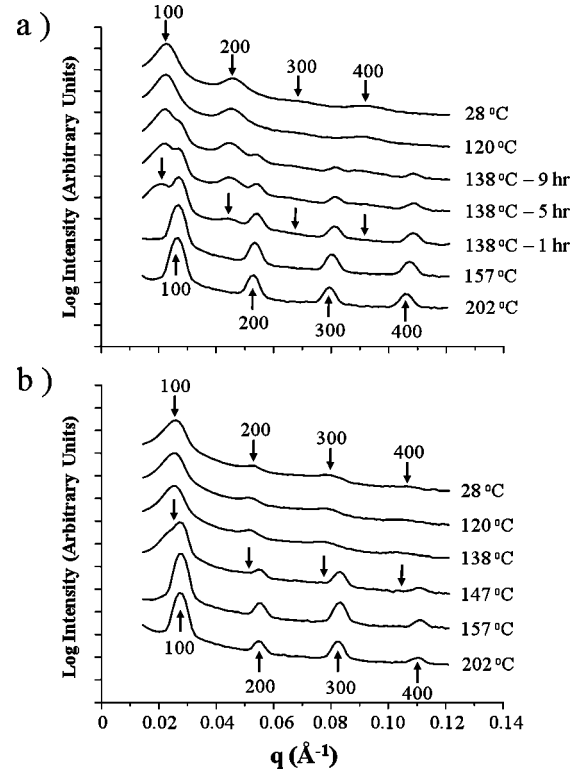

Figure 1. In-situ SAXS profiles as a function of temperature and annealing time. (a) $LiClO_4$-doped and (b) $LiCF_3SO_3$-doped PS−PEO ([EO]:[Li] = 3:1). Samples were prepared in an argon glovebox. Then, they were held in the SAXS under vacuum and at temperature for 1 h prior to data acquisition, except as noted in the figure. The diffraction peaks are identified by their Miller indices, where the 100 peak is designated as q^*. Data show temperature-dependent lamellar-to-lamellar OOT. Curves are shifted vertically for clarity.

10.1021/ma8014068 CCC: $40.75
Published on Web 08/16/2008

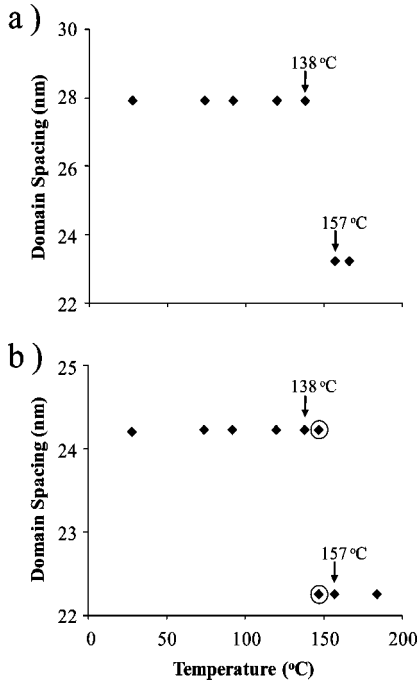

Figure 2. Domain spacing vs temperature calculated from the in situ SAXS data presented in Figure 1 for (a) $LiClO_4$-doped and (b) $LiCF_3SO_3$-doped PS−PEO ([EO]:[Li] = 3:1). Note the discontinuity in domain spacing as the polymer−salt complexes pass through the order−order phase transition. Also, note the coexistence of the two lamellar domain spacings for the circled data points at 147 °C.

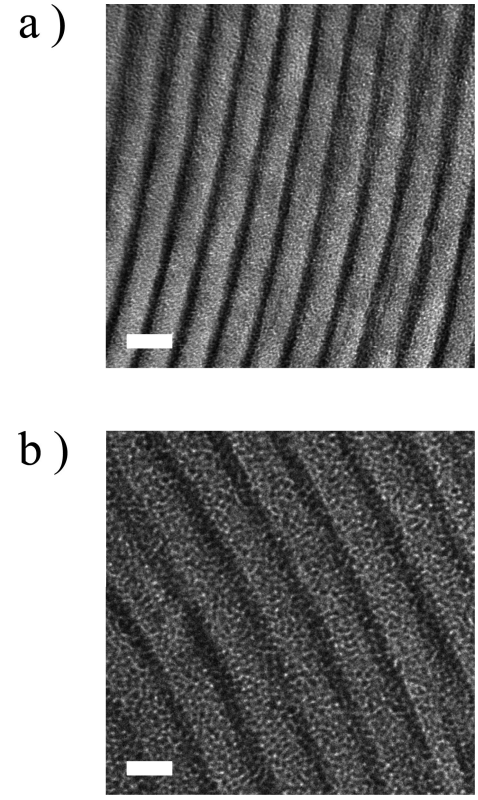

Figure 3. TEM micrographs of $LiClO_4$-doped PS−PEO ([EO]:[Li] = 3:1) after thermal annealing at (a) 166 °C and (b) 120 °C. Samples were cooled from 202 °C and then annealed for 12 h in the SAXS instrument, followed by quenching to room temperature. Thin sections with 70 nm thickness were obtained using a cryo-ultramicrotome at −60 °C and then collected on the 400 mesh copper TEM grids. PEO domains were darkened by RuO_4 staining. The scale bar represents 20 nm.

lamellar structure to another lamellar structure (with a larger domain spacing) has occurred upon cooling. The first (higher temperature) structure is recovered upon heating the sample above 157 °C.

A similar trend is found in the PS−PEO:$LiCF_3SO_3$ samples (Figure 1b). In this case, the order−order transition (OOT) appears to occur over a slightly faster time frame; however, the kinetics of this transition were not studied in detail. An intermediate temperature trace at 147 °C shows the growth of the series of scattering peaks at smaller q, as highlighted by arrows. Again, the first set of peaks was recovered upon heating above 157 °C. Additionally, though the T_{ODT}'s were not accessed during our experiments on either the PS−PEO:$LiClO_4$ or the PS−PEO:$LiCF_3SO_3$, the existence of Bragg reflections at temperatures up to 202 °C (the upper limit of our temperature experiments) suggests that T_{ODT} was significantly increased relative to the neat copolymer.[22,23,25]

Figure 2 shows the domain spacing ($d^* = 2\pi/q^*$) as a function of temperature obtained from Figure 1, where we note the discontinuity in domain spacing between 157 and 138 °C. For the $LiClO_4$-doped sample (Figure 2a), d^* increases from 23.3 to 27.9 nm across this transition, and a similar trend is observed for the $LiCF_3SO_3$-doped sample (Figure 2b), as d^* increases from 22.3 to 24.2 nm. The reversibility of this change in characteristic length scale is confirmed upon heating. Data at 147 °C (circled in Figure 2b) illustrate the transient coexistence of the two structures, indicating that they are two distinct phases. Longer annealing times show that the lower temperature phase is stable at 147 °C.

The existence of the two lamellar structures was confirmed by TEM. Micrographs for PS−PEO:$LiClO_4$ are shown in Figure 3. Both the higher and lower temperature lamellar structures were obtained by quenching SAXS samples to room temperature. The higher and lower temperature structures have d^* of 17 and 23 nm, respectively. Though the values calculated from TEM are lower than those from SAXS, the trend in domain spacing is corroborated. The discrepancy between SAXS and TEM values likely results from the SAXS acquisition temperature relative to TEM imaging temperature or the TEM micrograph angle. However, the magnitude of the TEM domain spacings, relative to SAXS, indicates that the samples were not significantly swollen by moisture during cryo-microtoming.

DSC was performed to locate $T_{m,PEO/Li}$ for the PEO−lithium complexes. Second heating curves are shown in Figure 4 for PS−PEO:$LiClO_4$ and PS−PEO:$LiCF_3SO_3$. The melting peak is distinct in each case, 139 °C (PEO−$LiClO_4$) and 157 °C (PEO−$LiCF_3SO_3$), and both $T_{m,PEO/Li}$ lie within the discontinuous domain spacing regions in Figures 1 and 2. Thus, it appears that crystallization of the PEO−salt complexes leads to the lamellar-to-lamellar phase transitions noted in the SAXS and TEM results. If transport in crystalline PEO materials becomes practical,[27] this transition could prove useful for increasing copolymer ordering and lamellar grain size. To confirm that the lithium salts existed solely within the PEO domains, the $T_{m,PEO/Li}$ in our nanostructured materials are compared to the melting temperatures of salt-containing PEO homopolymer.[29] Using homopolymer/salt melting temperature data and also accounting for the maximum EO/Li crystallite size in the copolymer[23,29,33] (estimated from domain spacings in Figure 2) yields $T_{m,PEO/Li}$ of 135 °C (PEO−$LiClO_4$) and 158 °C (PEO−$LiCF_3SO_3$). These calculated temperatures agree with our DSC values, indicating that the salt remains entirely within

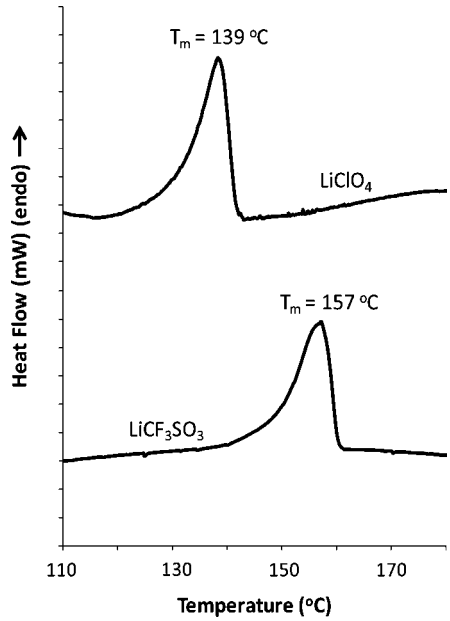

Figure 4. Second heating DSC curves for (a) $LiClO_4$-doped and (b) $LiCF_3SO_3$-doped PS-PEO ([EO]:[Li] = 3:1). Melting peaks are shown, and melting temperatures are identified. First and second heating and cooling cycles were run from −60 to 200 °C, and the heating rates were 10 °C/min. Curves are shifted vertically for clarity.

the PEO. Also, no melting peak for pure PEO was found in our samples.

One advantage of the PEO/Li system is that we can accurately determine the amount of salt present in the PEO domains and thus directly calculate the impact of salt concentration and PEO/Li complex formation on PS−PEO phase behavior. For both high salt complexes described in this work, we find that d^* increases discontinuously at $T_{m,\,PEO/Li}$. We can monitor the relative compositions of the crystalline and noncrystalline regions in the samples through SAXS without locating any intermediate states, indicating that crystallization likely causes a jump in d^* by promoting chain stretching and greater phase separation at the PS−PEO interface.[10] We note that this lamellar-to-lamellar order−order transition occurs above the glass transition temperature of the PS block.[34] Normally, one might expect that crystallization of this PS−PEO copolymer would lead to a disruption of the lamellar microstructure that exists at high temperatures (above the PEO/salt complex melting temperature),[35−37] with several exceptions.[10,38,39] We find that upon cooling crystallization is confined within the previously established lamellar motif with no breakout crystallization, likely a result of the increase in segregation strength upon doping.[40,41]

In future work, we will detail the systematic effects of adding lithium salts with various counterions to PS−PEO. Thus, we can determine the direct effect of cation concentration and counterion chemistry on the interaction parameters in PS−PEO copolymers. Given the differences in d^* for the two salts described herein, we expect to find differences in both the magnitude of the interaction parameters as a function of salt counterion as well as the parameters' dependence on temperature. We will correlate this behavior to the strength of the interactions between the lithium cation and its corresponding anions.

Acknowledgment. This work was supported by the ACS through Grant PRF-46864-67. We thank the Delaware Biotechnology Institute (DBI) for assistance in purchasing the Rigaku small-angle X-ray scattering instrument. This research program made use of the W.M. Keck Microscopy Facility at the University of Delaware. We thank Maeva Tureau, Frank Kriss, and Dr. Chaoying Ni for assistance with electron microscopy. We also thank Ghulam Hassnain Jaffari and Dr. John Rabolt for permitting usage of their calorimetry facilities. We acknowledge Dr. Bryan Vogt for helpful discussions.

References and Notes

(1) Gray, F. M. *Solid Polymer Electrolytes. Fundamentals and Technological Applications*; Wiley-VCH: New York, 1991; p 245.
(2) Ratner, M. A.; Shriver, D. F. *Chem. Rev. (Washington, DC, U.S.)* **1988**, *88* (1), 109–24.
(3) Abouimrane, A.; Alarco, P.-J.; Abu-Lebdeh, Y.; Davidson, I.; Armand, M. *J. Power Sources* **2007**, *174* (2), 1193–1196.
(4) Scrosati, B. *Chem. Rec.* **2001**, *1* (2), 173–181.
(5) Tarascon, J. M.; Armand, M. *Nature (London)* **2001**, *414* (6861), 359–367.
(6) Minier, M.; Berthier, C.; Gorecki, W. *J. Phys. (Paris)* **1984**, *45* (4), 739–744.
(7) Shi, J.; Vincent, C. A. *Solid State Ionics* **1993**, *60* (1−3), 11–17.
(8) Lascaud, S.; Perrier, M.; Vallee, A.; Besner, S.; Prud'homme, J.; Armand, M. *Macromolecules* **1994**, *27* (25), 7469–7477.
(9) Angell, C. A.; Liu, C.; Sanchez, E. *Nature (London)* **1993**, *362* (6416), 137–139.
(10) Hamley, I. W. Crystallization in block copolymers. In *Interfaces Crystallization Viscoelasticity*; Springer: Berlin, 1999; Vol. 148, pp 113−137.
(11) Bailey, T. S.; Pham, H. D.; Bates, F. S. *Macromolecules* **2001**, *34* (20), 6994–7008.
(12) Zhu, L.; Mimnaugh, B. R.; Ge, Q.; Quirk, R. P.; Cheng, S. Z. D.; Thomas, E. L.; Lotz, B.; Hsiao, B. S.; Yeh, F. J.; Liu, L. Z. *Polymer* **2001**, *42* (21), 9121–9131.
(13) Cho, B. K.; Jain, A.; Gruner, S. M.; Wiesner, U. *Science* **2004**, *305* (5690), 1598–1601.
(14) Epps, T. H., III; Cochran, E. W.; Bailey, T. S.; Waletzko, R. S.; Hardy, C. M.; Bates, F. S. *Macromolecules* **2004**, *37*, 8325–8341.
(15) Niitani, T.; Shimada, M.; Kawamura, K.; Kanamura, K. *J. Power Sources* **2005**, *146* (1−2), 386–390.
(16) Ionescu-Vasii, L. L.; Garcia, B.; Armand, M. *Solid State Ionics* **2006**, *177* (9−10), 885–892.
(17) Kim, S. H.; Misner, M. J.; Yang, L.; Gang, O.; Ocko, B. M.; Russell, T. P. *Macromolecules* **2006**, *39* (24), 8473–8479.
(18) Munch Elmér, A.; Jannasch, P. *Solid State Ionics* **2006**, *177* (5−6), 573–579.
(19) Bang, J.; Kim, B. J.; Stein, G. E.; Russell, T. P.; Li, X.; Wang, J.; Kramer, E. J.; Hawker, C. J. *Macromolecules* **2007**, *40* (19), 7019–7025.
(20) Djurado, D.; Curtet, J. P.; Bée, M.; Michot, C.; Armand, M. *Electrochim. Acta* **2007**, *53* (4), 1497–1502.
(21) Singh, M.; Odusanya, O.; Wilmes, G. M.; Eitouni, H. B.; Gomez, E. D.; Patel, A. J.; Chen, V. L.; Park, M. J.; Fragouli, P.; Iatrou, H.; Hadjichristidis, N.; Cookson, D.; Balsara, N. P. *Macromolecules* **2007**, *40* (13), 4578–4585.
(22) Epps, T. H.; Bailey, T. S.; Pham, H. D.; Bates, F. S. *Chem. Mater.* **2002**, *14* (4), 1706–1714.
(23) Epps, T. H.; Bailey, T. S.; Waletzko, R.; Bates, F. S. *Macromolecules* **2003**, *36* (8), 2873–2881.
(24) Wang, J. Y.; Chen, W.; Roy, C.; Sievert, J. D.; Russell, T. P. *Macromolecules* **2008**, *41* (3), 963–969.
(25) Ruzette, A.-V. G.; Soo, P. P.; Sadoway, D. R.; Mayes, A. M. *J. Electrochem. Soc.* **2001**, *148* (6), A537–A543.
(26) Lee, D. H.; Kim, H. Y.; Kim, J. K.; Huh, J.; Ryu, D. Y. *Macromolecules* **2006**, *39* (6), 2027–2030.
(27) Staunton, E.; Andreev, Y. G.; Bruce, P. G. *Faraday Discuss.* **2007**, *134*, 143–156.
(28) Fetters, L. J.; Lohse, D. J.; Richter, D.; Witten, T. A.; Zirkel, A. *Macromolecules* **1994**, *27* (17), 4639–47.
(29) Robitaille, C. D.; Fauteux, D. *J. Electrochem. Soc.* **1986**, *133* (2), 315–325.
(30) Chandrasekhar, V. *Adv. Polym. Sci.* **1998**, *135*, 139–205.
(31) Jacobs, P. W. M.; Lorimer, J. W.; Russer, A.; Wasiucionek, M. *J. Power Sources* **1989**, *26* (3−4), 503–10.
(32) Park, M. J.; Nedoma, A. J.; Geissler, P. L.; Balsara, N. P.; Jackson, A.; Cookson, D. *Macromolecules* **2008**, *41* (6), 2271–2277.
(33) Weimann, P. A.; Hajduk, D. A.; Chu, C.; Chaffin, K. A.; Brodil, J. C.; Bates, F. S. *J. Polym. Sci., Part B: Polym. Phys.* **1999**, *37*, 2053–2068.

(34) Huang, P.; Zhu, L.; Guo, Y.; Ge, Q.; Jing, A. J.; Chen, W. Y.; Quirk, R. P.; Cheng, S. Z. D.; Thomas, E. L.; Lotz, B.; Hsiao, B. S.; Avila-Orta, C. A.; Sics, I. *Macromolecules* **2004**, *37* (10), 3689–3698.
(35) Lee, W.; Chen, H. L.; Lin, T. L. *J. Polym. Sci., Part B: Polym. Phys.* **2002**, *40* (6), 519–529.
(36) Quiram, D. J.; Register, R. A.; Marchand, G. R.; Ryan, A. J. *Macromolecules* **1997**, *30* (26), 8338–8343.
(37) Schmalz, H.; Knoll, A.; Mueller, A. J.; Abetz, V. *Macromolecules* **2002**, *35* (27), 10004–10013.
(38) Hong, S.; MacKnight, W. J.; Russell, T. P.; Gido, S. P. *Macromolecules* **2001**, *34* (9), 2876–2883.
(39) Floudas, G.; Vazaiou, B.; Schipper, F.; Ulrich, R.; Wiesner, U.; Iatrou, H.; Hadjichristidis, N. *Macromolecules* **2001**, *34* (9), 2947–2957.
(40) Loo, Y. L.; Register, R. A.; Ryan, A. J. *Macromolecules* **2002**, *35* (6), 2365–2374.
(41) Xu, J. T.; Fairclough, J. P. A.; Mai, S. M.; Chaibundit, C.; Mingvanish, M.; Booth, C.; Ryan, A. J. *Polymer* **2003**, *44* (22), 6843–6850.

MA8014068